Catalysis Today xxx (2012) xxx–xxx

Contents lists available at SciVerse ScienceDirect

Catalysis Today

journal homepage: www.elsevier.com/locate/cattod

Nickel supported on zinc oxide nanowires as advanced hydrodesulfurization catalysts

Franz G. Petzold[a,c], Jacek Jasinski[a], Ezra L. Clark[a,b], Jeong H. Kim[a,b], Jason Absher[a], Helge Toufar[c], Mahendra K. Sunkara[a,*]

[a] Department of Chemical Engineering and Conn Center for Renewable Energy Research, University of Louisville, Louisville, KY 40292, United States
[b] Advanced Energy Materials, LLC., 201 E. Jefferson Street, Suite 303, Louisville, KY 40202, United States
[c] Sud-Chemie, Inc., 1600 Hill Street, Louisville, KY 40210, United States

ARTICLE INFO

Article history:
Received 16 February 2012
Received in revised form 7 May 2012
Accepted 10 May 2012
Available online xxx

Keywords:
Zinc oxide nanowires
Hydrodesulfurization
Reactive adsorption
Atmospheric plasma jet reactor
Ni impregnation

ABSTRACT

A novel catalyst with deep hydrodesulfurization (HDS) capabilities was tested with the aim of producing ultra-low sulfur diesel oil. The catalyst consisted of a zinc oxide nanowire (ZnO NW)/alumina carrier impregnated with nickel (Ni) as the active phase. Based on the concept of reactive adsorption, it was hypothesized that enhanced metal–support interactions and short diffusion paths between Ni and ZnO NWs could lead to improved activity and sulfur uptake capacity. Long ZnO NWs (10–15 μm) were produced in bulk quantities using an atmospheric plasma jet reactor. In situ heating studies of Ni impregnated ZnO NW samples revealed better Ni dispersion, greater Ni-support interaction, and smaller Ni particle sizes when compared to a support comprised spherical ZnO nanoparticles (NPs). The reactive adsorbent was tested for on-stream sulfur uptake with model diesel oil spiked with difficult-to-remove organic sulfur species. The data indicated high activity for deep de-sulfurization in the initial stages but the catalyst deactivated via coking after 16 h. The coking appears to be due to cracking of aromatic species present in the model oil in the absence of adsorbed surface hydrogen. The initial activity of the catalyst with modest composition of nickel loading indicated the potential utility of the catalyst system involving ZnO NWs as support.

1. Introduction

The reduction of sulfur content in gasoline and diesel oil is an important means for improving air quality because of the negative impact sulfur has on the performance of automotive engine exhaust inhibitors as it irreversibly poisons noble metal catalysts in the converter. Aside from the legislative pressure, the demand for ultra-low sulfur fuels has also naturally been driven by the growing application of fuel cells. Due to their high energy density, ease of storage, and well-established distribution-infrastructure, transportation fuels such as gasoline, jet fuel, and diesel oil are perfect candidates for high efficiency fuel cells. Nevertheless, to protect the reforming catalyst and the electrodes of the fuel cell system from deactivation, the sulfur concentration of the fuel needs to be ultra-low (<0.1 ppm). In light of the legislative developments to prevent emissions of sulfur oxides as well as the general emergence of ultra-low sulfur applications, ultra-deep desulfurization of gasoline and diesel oil has become an increased focus of research with many diverse approaches.

Conventional HDS utilizes alumina- and silica-supported cobalt or nickel molybdenum catalysts. However, even though significant improvements in decreasing sulfur content have been made, it is still difficult to achieve completely sulfur free fuels, which is mostly due to slow reactivities of sterically hindered dimethyl dibenzothiophenes [1–5]. The reactive adsorption system presented in this paper aims at removing thiophene based compounds (such as those shown in Fig. S1) from conventionally treated HDS streams.

1.1. Catalysts for conventional hydrodesulfurization

Typical catalysts for hydrogenation and conventional HDS are transition metals of the Groups-9 and -10 elements, displaying vacant d-orbitals such as cobalt ($3d^7$), nickel ($3d^8$), rhodium ($4d^8$), palladium ($4d^{10}$), and platinum ($5d^9$). Ni and cobalt (Co) with various promoters and on various supports are extensively used. Carbon–heteroatom cleavage under hydrogen pressure is achieved via a classical hydrogenolysis reaction scheme. Extensive studies on catalytic properties of transition metal catalysts showed that Ni and

* Corresponding author. Tel.: +1 502 8528574; fax: +1 5028526355.
E-mail address: mahendra@louisville.edu (M.K. Sunkara).

0920-5861/$ – see front matter © 2012 Elsevier B.V. All rights reserved.
http://dx.doi.org/10.1016/j.cattod.2012.05.030

Co have the best catalytic activity [9–14]. Conventional catalysts like Co(Ni)–Mo/Al_2O_3 achieve bulk sulfur removal from gasoline and natural gas with residual organo-cyclic sulfur compositions down to 30 wt ppm [15]. In a hydrogen atmosphere, the metal active phase, i.e. nickel, is able to cleave the sulfur off the "difficult" cyclic compounds; thereby converting the sulfur into hydrogen sulfide (H_2S). Nonetheless, the active nickel phase is slowly sulfided by the resulting H_2S forming NiS according to the following reaction:

$$Ni + H_2S \rightarrow NiS + H_2 \quad \Delta G(500\,K) = -42.3\,kJ/mol \tag{1}$$

As nickel undergoes conversion to NiS, the adsorption activity decreases and eventually vanishes completely. In industry, the catalyst will either have to be regenerated or replaced once a certain threshold breakthrough of sulfur is detected in the product stream. There are several actively researched alternative methods which aim at removing sulfur to levels below 10 ppm. Song, Ito et al. and Stanislaus et al. summarized the most prominent research areas, including oxidative routes for diesel, chemical conversion methods, non-destructive adsorption, extraction, biodesulfurization, and, subject of this paper, reactive adsorption [5–8]. The concept behind reactive adsorption is that once a conventional metal active phase of a catalyst converts all "difficult" organic sulfur species under hydrogen to H_2S, an adsorptive phase, usually the base oxide support material, accepts and permanently stores the sulfur portion of the H_2S. The permanent storage capacity is important, as H_2S, when present downstream of the catalyst adsorbent, tends to recombine with olefins to relatively stable mercaptanes.

1.2. The reactive adsorption catalyst concept using ZnO NWs as support

The active surface nickel can catalyze the cleaving of cyclic sulfur compounds such as thiophenes. During the process, however, the active Ni sites get sulfided to NiS thereby extinguishing catalytic activity. A proper ZnO support can ensure that active nickel phase is present during deep desulfurization through the following regenerative step.

$$NiS + ZnO + H_2 \rightarrow Ni + ZnS + H_2O \quad \Delta G(500\,K) = -32.2\,kJ/mol \tag{2}$$

In this study, we investigated the concept of reactive adsorption, utilizing ZnO NWs as catalyst support, to maintain a steady fraction of active Ni surface sites for ultra-deep HDS. See Fig. 1 for schematic illustration. The catalytic activity can, hence, be extended until all accessible ZnO is completely converted to ZnS. The reactive adsorption system studied here is intended for ultra-deep HDS i.e. polishing off the difficult to remove thiophenes that are still present in conventionally processed HDS streams down to zero ppm (from 20 to 50 ppm). Several research groups have carried out investigations to develop an understanding of the mechanism of the desulfurization process via reactive adsorption [15–23]. A recent report suggests sulfur transfer to ZnO through Ni_3S_2 under desulfurization tests [24]. Although the HDS process is more effective with a pure Ni catalyst, the sulfiding of the Ni surface to form NiS ultimately reduces the life of the catalyst. Tawara et al. tested a Ni/ZnO catalyst for hydrodesulfurizing kerosene which allowed for reducing sulfur levels below 0.1 wt ppm [22,25]. The operational time scales for feed streams with sulfur levels below 50 ppm and 35% sulfur uptake, using a reactive adsorption catalyst comprised 15% Ni on ZnO can exceed a 1000 h under conventional space velocities. During this period, the catalyst can maintain a steady fraction of surface Ni concentration for deep desulfurization.

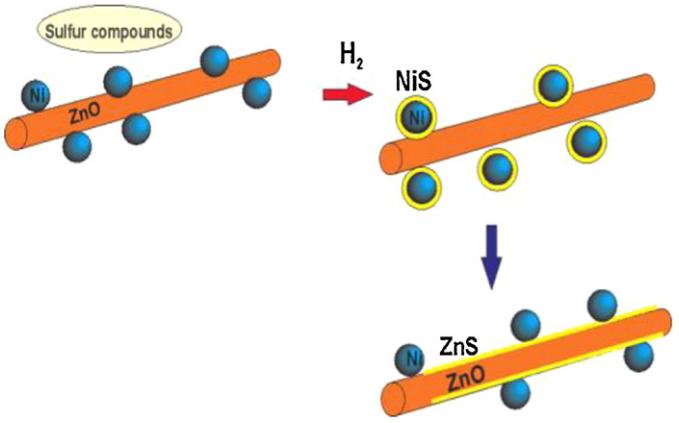

Fig. 1. A schematic illustration of reactive adsorption of thiophenic compounds on Ni decorated ZnO NW. ZnO NW support keeps Ni sites free of sulfur and thereby active for hydrogenolysis.

In addition to the reactivity aspect discussed above, the supports also play a key role for catalyst design for the following reasons: the active metal dispersion via size distribution, morphology, metal support interaction and non-sinterability for maintaining activity. Very recently, researchers have begun to study the use of ZnO nanorods as supports for Ni and Co particles and studied their performance at small laboratory scales with various reactions: hydrogen production using steam reforming of bioethanol [26] and desulfurization [23,27,19]. However, to the best of our knowledge, no studies exist for nanowire powders at pre-commercial level testing. This study reports first of its kind attempts to prepare and test catalysts using Ni supported on ZnO NW powders.

2. Experimental

2.1. Zinc oxide NW powder production

Bulk production experiments were performed using an atmospheric plasma jet based reactor as shown in schematic in Fig. 2 and described earlier [28]. In this reactor, micron scale zinc metal powders are supplied from the top using a powder sifter and the resulting zinc oxide nanomaterials are collected using a filter bag. Several studies were performed to optimize continuous production of ZnO NW powders. The feed powder consisted of Zn microparticles (1–45 μm). A feed rate of 1 g/min, a plasma power of 1 kW, O_2 flow rate of 2.5 lpm, N_2 flow rate of 12.5 lpm were used respectively.

2.2. Nickel impregnation onto ZnO NW powders

Impregnation with nickel acetate (NiAc) solution was chosen to deliver the active Ni phase onto the ZnO NWs. The ZnO NW powder and NiAc hexahydrate were mixed for a target Ni:ZnO ratio of 3:7 using DI water and a small quantity of ammonium hydroxide solution. The pH was maintained at 9 and the mixture was ultrasonicated for 5 min to assure proper dispersion and exposure of the ZnO NWs. The suspension was dried by evaporating water at 95 °C. The resulting greenish flakey powder was calcined in air at 400 °C for 2 h. The calcined powder was loosely crushed in a mortar for X-ray diffraction (XRD) analysis using Bruker D8. The XRD pattern shown in Fig. S2 (supplementary document) shows the hexagonal wurtzite ZnO for nanowires and the face-centered cubic bunsenite phase for NiO crystals. The mean NiO particle size was estimated using XRD data to about 11 nm. Aside from the identification of the two desired phases, the Ni loading was also confirmed to be

Please cite this article in press as: F.G. Petzold, et al., Nickel supported on zinc oxide nanowires as advanced hydrodesulfurization catalysts, Catal. Today (2012), http://dx.doi.org/10.1016/j.cattod.2012.05.030

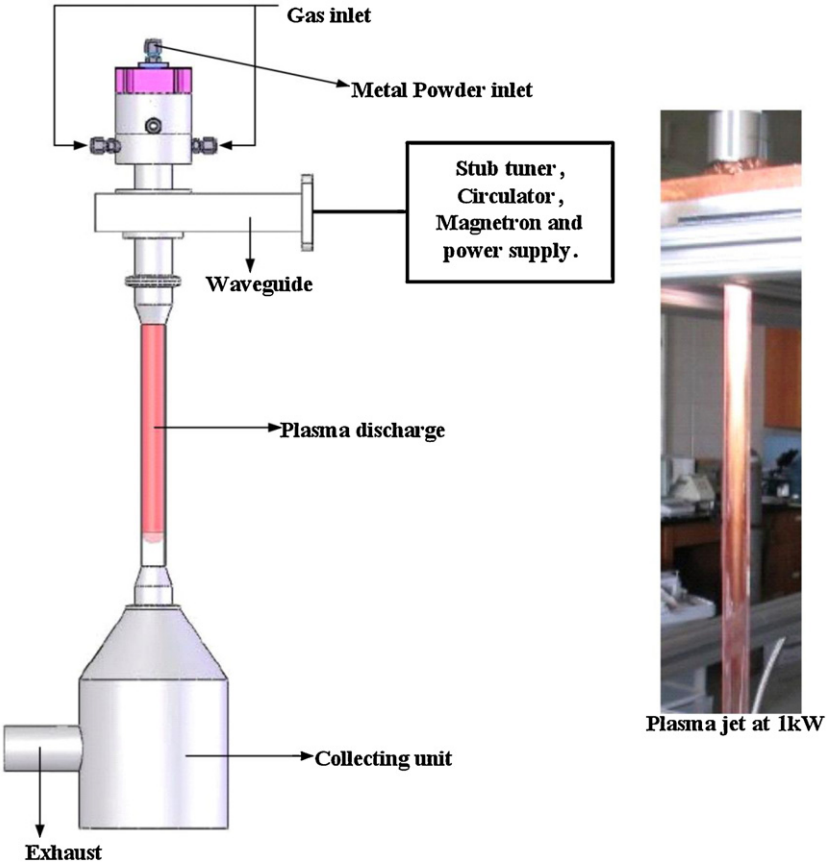

Fig. 2. Schematic and photograph of our microwave plasma jet reactor.

15 wt% NiO. The samples were supported on gold sputtered silicon substrates and examined using a field emission scanning electron microscope (FEI NanoSEM). At 15 wt%, the surface coverage of ZnO NWs with NiO was less than 50%. SEM images shown in Fig. S3 shown that the morphology of ZnO NWs after nickel impregnation is still intact.

2.3. Catalyst preparation

ZnO NW powder (10.28 g) was suspended in a 1 l beaker filled with de-ionized water and sonicated for 15 min. The suspension was allowed to settle for 20 min before the supernatant was vacuum-filtered through a paper filter with a 2.5 μm pore size. The filter with the attached wet filter cake was dried for 1 h at 110 °C, after which the dried ZnO NWs were collected from the filter. The final yield of high purity ZnO NW was 70% or 7.2 g. For a target weight composition of 64:20:16 ($ZnO:Al_2O_3$:Ni), 5.84 g of the high quality product was mixed with 1.82 g of γ-alumina and 6.35 g of NiAc. The product mixture was suspended in 250 ml of de-ionized water and ultra-sonicated for 8 min to re-disperse the ZnO NW filter cake flakes. The beaker with the pale green suspension was put in a furnace at 80 °C over night. Once 150 ml of water were evaporated, the resulting creamy substance was further heated to 150 °C with occasional stirring. The final 40 ml were thick enough to extrude the dough into extrusions, which were then dried over night at 70 °C. The final drying temperature was ramped up to 250 °C at 1°/min. rate. The product extrusions became darker but stayed greenish until they were calcined at 400 °C for 2 h, at which point they almost immediately turned dark gray. After a cool-down period, the extrusions were sized to five by 2 mm pieces of which 10 ml were measured out for testing.

2.4. Desulfurization studies

The testing was done using a model hydrocarbon stream spiked with an assortment of aforementioned "difficult" aromatic sulfur species in a setting that closely resembles industry conditions. It seemed appropriate to employ a diesel feed that contained aromatics to see if the catalyst also conveyed a noticeable level of regular hydrogenation activity. A standard diesel feed was acquired from Exxon containing 25% of various aromatic and poly-aromatic compounds. The sulfur content of 20 ppm consisted mostly of thiophene (10 ppm), benzo-thiophene (3 ppm), di-benzo-thiophene (3 ppm), and a few moderately and severely sterically hindered di-benzo-thiophenes. The final catalyst extrusions were diluted with SiC (7:1) and loaded in a fixed bed reactor. The NiO particles were reduced to metallic Ni using 1 l/min hydrogen flow over the bed at 430 °C for 16 h.

For testing, the hydrogen flow rate was set at 0.098 l/min at a pressure of 435 psi g, the reactor heaters fired at 190 °C, and the diesel pump rate was set to 0.5 ml/min, which, relative to the superficial volume of the catalyst extrusions (10 ml), translated into a liquid hourly space velocity (LHSV) of 3 h^{-1}. Product samples were collected for every 4 h.

Temperature programmed reduction (TPR) runs were conducted on NiO decorated ZnO NWs to study the sintering susceptibility of the NiO/ZnO NW system compared to NiO supported on commercial ZnO NPs. The two samples were loaded with 20% Ni (from acetate) and reduced in a nitrogen stream with five

Please cite this article in press as: F.G. Petzold, et al., Nickel supported on zinc oxide nanowires as advanced hydrodesulfurization catalysts, Catal. Today (2012), http://dx.doi.org/10.1016/j.cattod.2012.05.030

percent hydrogen on a Micromeritics Autochem II 2920. The ramp rate of the reduction was 10 °C/min and the hydrogen consumption signal was recorded from 30 °C to 500 °C.

The surface area of a plain ZnO NW sample was measured via the Brunauer–Emmett–Teller (BET) method using nitrogen at 77 K on a vacuum volumetric gas-sorption Micromeritics TriStar 3000.

3. Results and discussion

3.1. Bulk production of ZnO NW powders

There has been a tremendous amount of research in NW synthesis method development, evidenced by the explosion in papers published in the last 15 years. Much of the work utilized clusters of gold or other catalytic metals (Ni or iron) to catalyze the growth via vapor–liquid–solid (VLS) approaches [29,30]. In the VLS mechanism, each metallic cluster catalyzes dissolution of gas phase solutes and precipitates the solute or its compounds in one-dimensional form [31]. In the above approach, a large quantity of nanoscale catalytic metal clusters with well-controlled sizes is required for producing NWs. Besides, the use of precious metals such as gold is not practical for large-scale synthesis due to cost and rarity. The use of iron is promising, but requires high temperatures in excess of 900 °C and has not been demonstrated with continuous production schemes yet. There have been several interesting routes developed for synthesizing one-dimensional materials without using the above group of metals [32,33]. In this case, high density of semiconductor NWs can nucleate and grow from micron-sized clusters of low-melting metals [31,32]. Similarly, the oxide or similar compounds of low-melting metals NWs could be synthesized directly without the use of foreign metal clusters [34–36]. In the schemes involving self-catalyzed or direct reaction, there is no foreign metal involved as a contaminant. Traditionally, the formation of nanoparticles (NPs) is easier and, irrespective of the method used (flame, laser, hot wall, and plasma reactor), the mechanism involves rapid nucleation followed by arrested growth via short residence times in hot reacting zone [37]. However, the same concept cannot be applied in the case of NWs where the synthesis must be able to preferentially support growth in one dimension, thus making NW production difficult compared to that of NPs. Many researchers exploited the use of catalysts to grow 1-D structures using substrates in a number of approaches such as thermal evaporation [37], laser ablation [30], hydrothermal synthesis [38], electrodeposition [39], and others. However, no reports exist on scale-up or large-scale production of NW powders.

Earlier studies showed that synthesis of tin oxide and zinc oxide nanowires is possible using oxidation of respective metal powders using atmospheric plasma jet [28]. Here, several experiments are performed to optimize the conditions, powder feed rate and collection method for developing a scheme for hundred gram scale production of ZnO NW powders. Synthesis of the ZnO NWs was accomplished using an applied microwave power of 1 kW, an overall gas flow rate of 15 lpm, and a raw feed rate of 1 g/min. The gas phase composition consisted of a mixture of N_2, O_2, and H_2 with an overall O_2 concentration of 2–20% and an H_2 flow of 0–500 sccm. Experiments conducted with lower O_2 percentages (<12%) resulted in low quality NWs (lengths of roughly 1 μm) and zinc metal contamination in the product powders. Higher oxygen ratios (>17.5%) resulted in roughly a gram of nanowire powders in 2 min with >90% purity. Experiments conducted with a raw feed of zinc NPs resulted in short NWs with lengths less than 1 μm, due to the metal source feeding the NW growth being depleted. Large raw feed particles (>20 μm in diameter) resulted in zinc metal contamination in the product powders, due to the inability of the plasma to convert the bulk of the metal particles to metal oxide. Based on these results, it was determined that the optimum raw feed particle size was between 1 and 5 μm.

The type of powder flow from the feeder in to the plasma zone had a major effect on the percent conversion and resulting nanowire characteristics. Agglomerated raw feed resulted in rapid sintering of the individual zinc metal particles, leading to the formation of relatively large zinc metal pebbles. Highly dispersed flow, with raw metal feed powders being showered into the reactor inlet, resulted in a significant improvement in the quality and purity of the resulting NW powders. This is probably due to rapid oxidation of dispersed powders while reducing the tendency of the raw feed particulates to sinter.

In all nanowire production experiments, the quartz tube wall received substantial deposition with ZnO powder. At the top of the reactor, near the source of the plasma flame, depositions consisted of mostly nanoparticles. This region of the deposition was also where the product mass was most densely concentrated. Downward, the deposition was thinner with morphology predominantly being one-dimensional in nature. At the base of the quartz tube nearly 50% of the deposition mass was accounted for by nanowires with lengths of roughly a micron.

In order to understand the stages of gas phase oxidation of zinc metal powders, samples were collected at different locations from the gas phase within our plasma reactor as shown in Fig. 3. The data shows various stages of nucleation and growth of zinc oxide nanowires from molten Zn particles. The first sample collected close to plasma zone shows multiple nucleation events from one molten Zn particle. The sample collected at later stages in the reactor showed longer, individual nanowires. The data proves that the Zn metal powder gets oxidized in the gas phase and nucleation and growth of ZnO nanowires result from oxidation of molten Zn particles in the gas phase.

The use of high surface area filters allowed for continuous production runs without causing pressure drop and disruption in production process. Continuous runs resulted in more than hundred grams of ZnO NW powders as shown in Fig. 4. Typical results show that the resulting NWs are typically 1–30 μm in length and diameters from 5 to 50 nm. The optimum plasma power for the synthesis was found to be 1 kW. At less than 1 kW powder no conversion of the Zn powder to ZnO NW was obtained. At powers higher than 1 kW, the Zn powder vaporized and no product was collected in the filter. Also using powders with particle size greater than 10 μm and feed rates higher than 1 g/min resulted in the agglomeration of the feed powders and lowered the conversion. No significant change in the conversion was found when oxygen flow rate was varied between 10 and 15 lpm. The observations of very long (>20 μm) and thin diameters (about 10 nm) for nanowires collected in the filter are surprising which suggest prolonged growth of nanowires entrained in gas phase after completely consuming the original metal cluster. Similarly, the SEM images of nanowire aggregates collected from filters indicate hairy ball type entanglements suggesting interesting aggregation patterns of thin and long nanowires in gas phase. Further studies are needed for understanding some of these observations.

3.2. In situ decomposition studies of Ni precursors on ZnO NWs

The nucleation and evolution of Ni particles on the ZnO NWs via decomposition of NiAc was studied in situ in a transmission electron microscope (TEM) using a heating sample holder. A drop of the suspension/solution (NiAc covered ZnO NWs) was dripped onto a carbon grid, dried, mounted in a furnace-type Gatan 628 Single Tilt Heating Holder, and loaded into a Tecnai F20 FEG TEM chamber for in situ TEM heating studies. At first, a suitable area of the grid with a few well-dispersed ZnO NWs was identified at room temperature. Then the sample was gradually heated with

Please cite this article in press as: F.G. Petzold, et al., Nickel supported on zinc oxide nanowires as advanced hydrodesulfurization catalysts, Catal. Today (2012), http://dx.doi.org/10.1016/j.cattod.2012.05.030

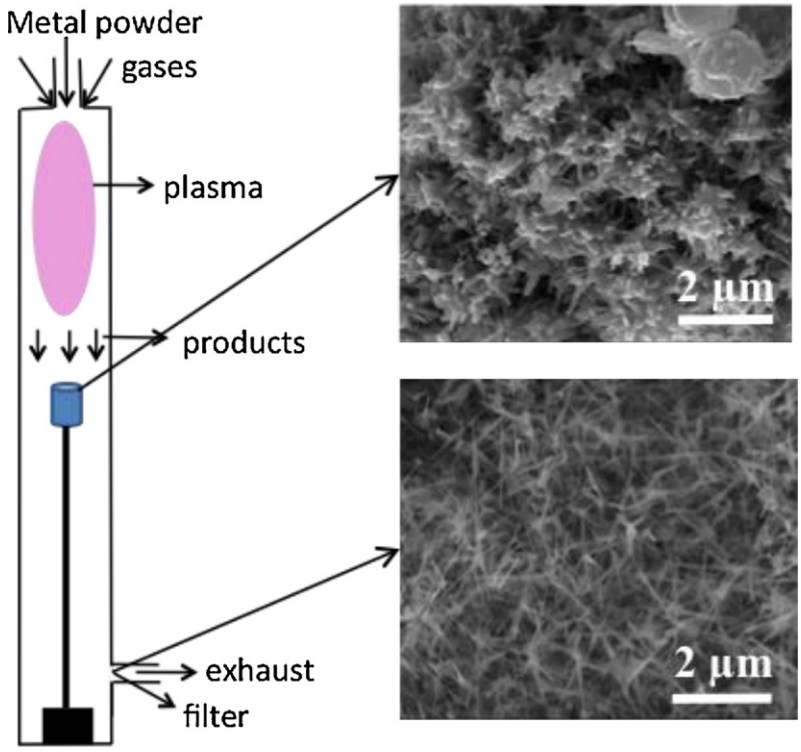

Fig. 3. SEM image of ZnO nanowire powders collected at two different locations within the plasma jet reactor as shown in the schematic.

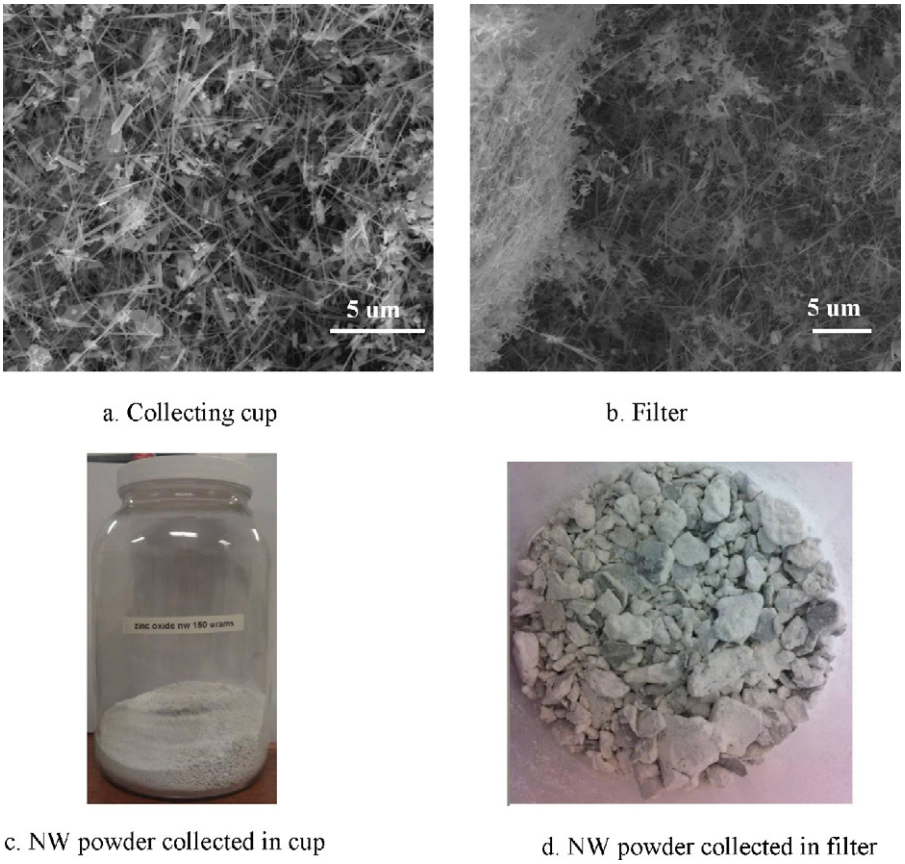

Fig. 4. SEM images and photographs of ZnO nanowire powders collected in cup at bottom and high surface area filter. The photographs of bottles containing ~150 g of ZnO NW powder collected in cup and 6 g of ultrafine NW powder (~5–20 nm dia.; >20 μm length).

Please cite this article in press as: F.G. Petzold, et al., Nickel supported on zinc oxide nanowires as advanced hydrodesulfurization catalysts, Catal. Today (2012), http://dx.doi.org/10.1016/j.cattod.2012.05.030

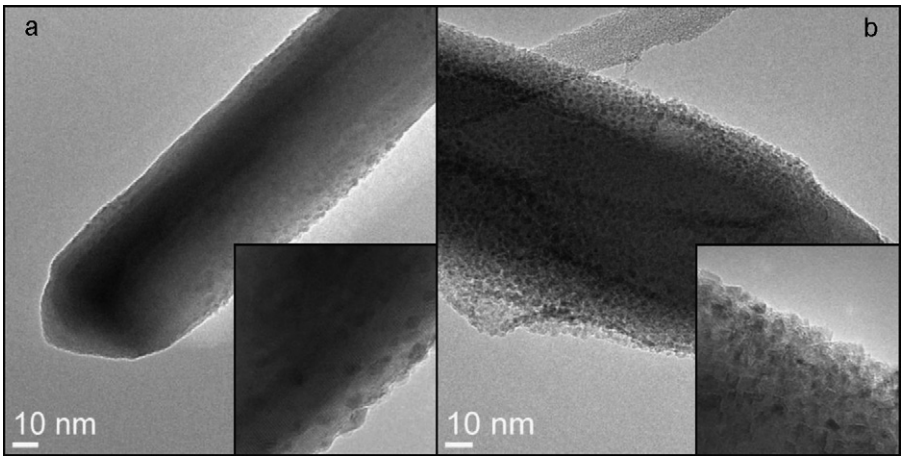

Fig. 5. TEM images of a Ni decorated ZnO NW after in situ decomposition of (a) NiAc at 430 °C, and (b) NiFt at 410 °C.

intervals of ~50 °C and at each subsequent temperature, after temperature stabilization (~5 min), TEM images were recorded from the selected area to monitor changes. The chamber was under high vacuum which prevented formation of NiO. At ~330 °C Ni nuclei started to emerge from the amorphous NiAc and the average size of formed Ni particles was gradually increasing with the heating temperature. As shown in Fig. 5a, after heating at final temperature of 430 °C, dispersion of Ni particles is very high with only very few and small agglomerations. Ni particles formed are quasi-spherical and their size averages around 30 Å, which is an excellent result and a good indicator for high catalytic activity. In addition to NiAc, we also studied nickel formate (NiFt) dihydrate as Ni precursor. In particular, we performed similar in situ thermal TEM decomposition studies and observed formation of Ni nuclei starting at ~370 °C. In this case, heating at ~410 °C, lead to the complete decomposition of the precursor and high dispersion of Ni particles on ZnO NWs (see Fig. 5b). Particles were found to be even smaller that in the NiAc sample (down to ~20 Å) and they exhibited a distinct cubic morphology. Also see Fig. S4 (supplementary document) for more images. A set of energy-dispersive X-ray spectroscopy (EDS) elemental maps, including maps of Ni, Z, and O, obtained from a single ZnO NW, confirmed that the NPs decorated onto the ZnO NWs are indeed NiO. For this, a freshly prepared and calcined NiO/ZnO NW sample was ultrasonicated in ethanol, dripped onto a copper grid, dried and loaded into the TEM chamber. The individual elemental maps, which are displayed in Fig. S5, unmistakably show how Ni is distributed in a form of particles and particle clusters over the NW.

TPR studies were performed to gain insight into the support-Ni particle interactions. A reference sample with a nickel loaded ZnO NP powder (surface area = 57 m^2/g, mean crystallite size = 17 nm) was prepared in the identical fashion as the ZnO NW sample. The TPR profiles (see Fig. 6) display one major peak which points to a relatively uniform nickel particle size distribution in the sample The ZnO NP reference sample showed a reduction maximum of 345 °C and the ZnO NW sample at 358 °C. The considerable difference between the reduction maxima implies that the NP sample with the lower reduction temperature shows relative ease of NiO reduction compared to the NW sample. Reducibility can serve as a measure of nickel-support interaction. The stronger the NiO interacts with the ZnO support the more difficult it is to reduce it to Ni. In addition, the stronger metal-support interaction correlates with smaller NiO and Ni particle sizes.

A hot stage XRD was conducted to gain insight into the Ni particle size evolution during reduction. An XRD pattern was recorded for every 25 °C increase in temperature at the same reduction conditions as the TPR runs. When the ZnO NP sample (which was reduced in the same manner) is taken as a reference, the ZnO NWs appear to reduce the extent of Ni sintering. Fig. S6 displays the mean crystallite size evolution during reduction of both Ni decorated ZnO NPs and ZnO NWs.

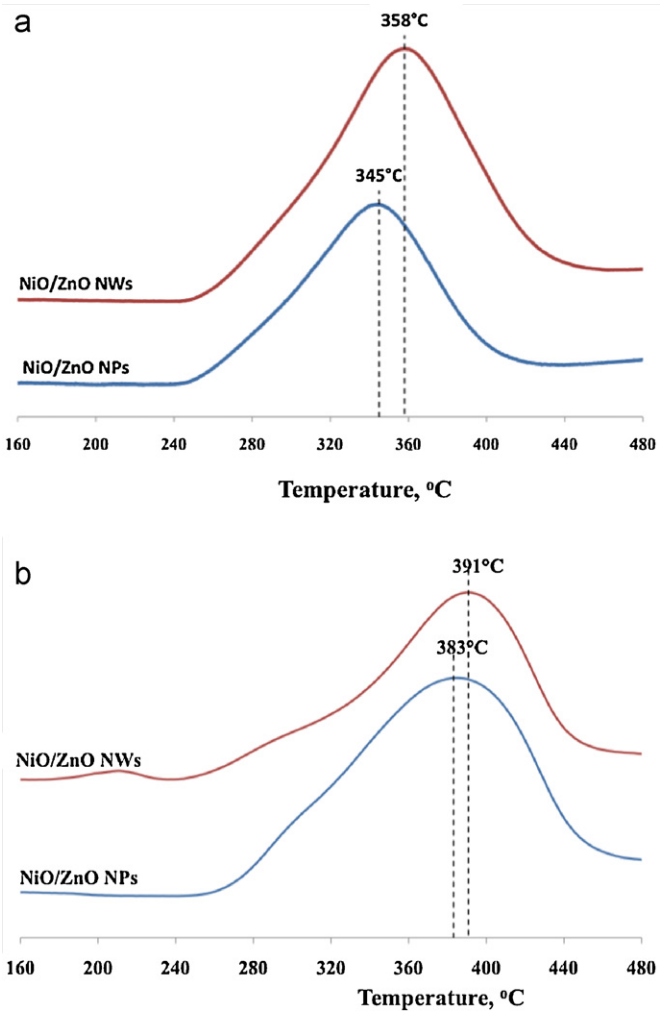

Fig. 6. TPR profiles of NiO supported on ZnO NWs and ZnO NPs. Ni–ZnO support interactions are stronger with NWs for both Ni precursors used (a) NiAc and (b) NiFt.

Please cite this article in press as: F.G. Petzold, et al., Nickel supported on zinc oxide nanowires as advanced hydrodesulfurization catalysts, Catal. Today (2012), http://dx.doi.org/10.1016/j.cattod.2012.05.030

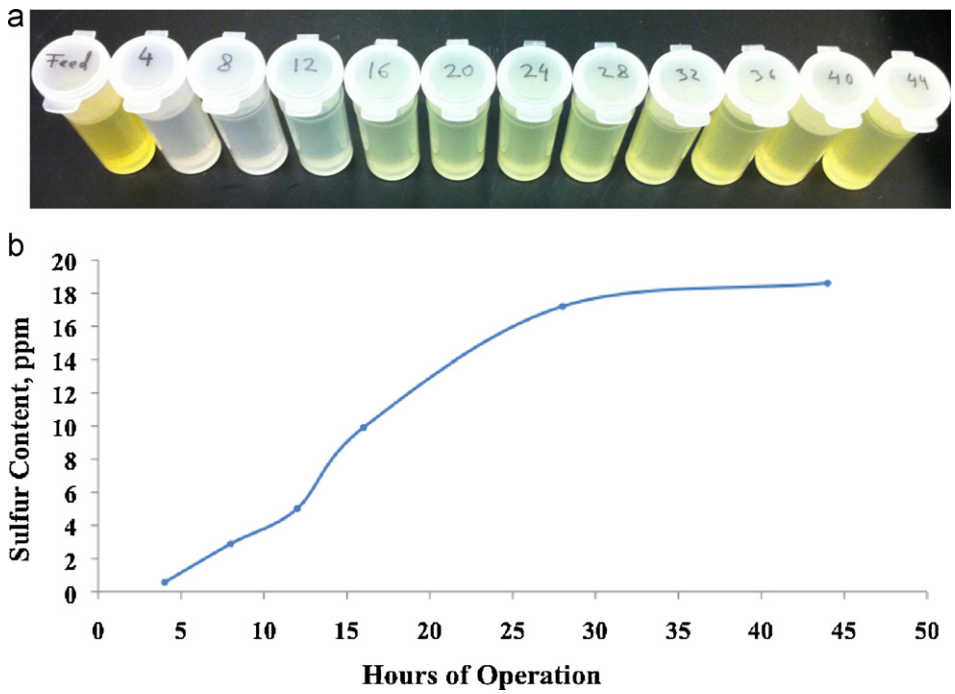

Fig. 7. Desulfurization test results of catalyst comprised 15% Ni, 20% γ-Al_2O_3, and 65% ZnO NW: (a) photographs of diesel samples taken at various time scales during testing; and (b) the quantification of sulfur content in the treated diesel.

Studies were also performed to investigate if the proposed catalyst carrier chemisorbs and stores hydrogen sulfide (H_2S). A ZnO NW powder sample of 0.2 g was turned into slurry with ethanol, spread onto a quartz plate, and placed in a vacuum reactor chamber. The reactor was slowly pumped down to a moderate 0.05 Torr and heated to 200 °C. A 25 sccm stream of H_2S was then flown over the sample for 14 h. As shown in Fig. S7, a following XRD analysis of the powder identified a cubic zinc sulfide (ZnS) phase. Quantification revealed that 38.2% of the sample is ZnS, and the 61.8% remainder is comprised ZnO. The SEM images of the sulfided sample appear to show "swelling" of the NWs; however, the general morphology is well maintained.

3.3. Ni impregnation of ZnO NWs

ZnO NWs were impregnated via a NiAc solution. A small quantity of ammonium hydroxide solution was added to maintain the overall solution pH at 9. The powder was dried and calcined at 400 °C. The SEM images of ZnO NWs impregnated with Ni using Ni Ac precursor are shown in Fig. S3. Analysis of the XRD patterns of Ni impregnated ZnO NWs sample shows both hexagonal wurzite ZnO and cubic phase of NiO. Utilizing the Scherrer equation, the average NiO crystallite size was found to be much less than 20 nm, which conforms to industry standards. To verify that the NiO particle size is less than 20 nm and to show that these particles are uniformly

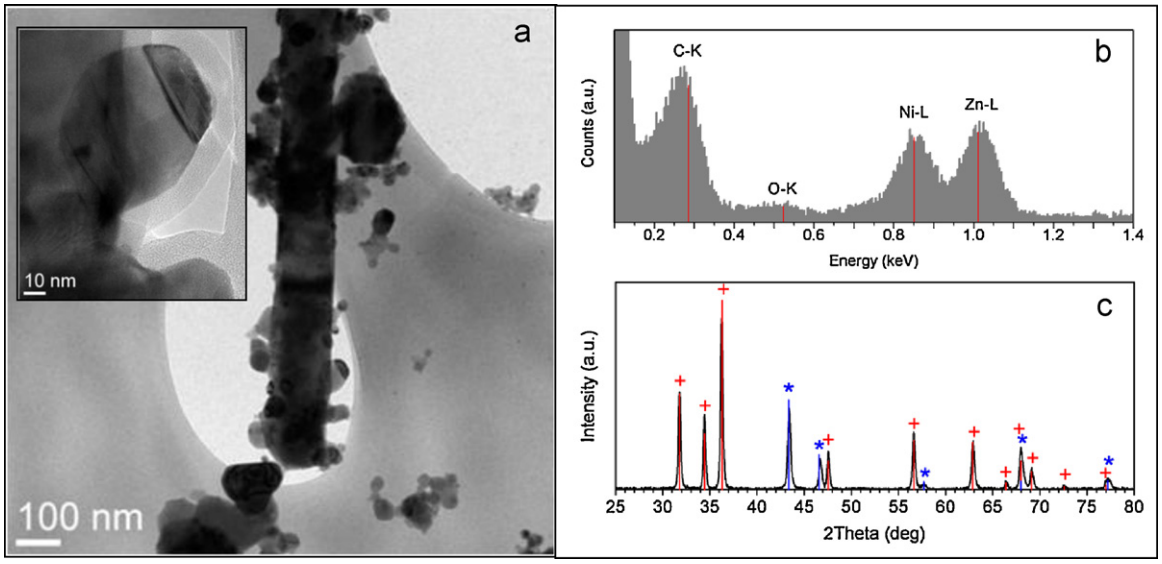

Fig. 8. (a) TEM image of spent Ni/ZnO NW sample from NiFt precursor. The inset shows a large NiZn particle covered with a thick carbon layer. (b) EDS–TEM spectrum obtained from a single NiZn particle. (c) XRD pattern measured from this sample showing ZnO (red crosses) and NiZn (blue stars) peaks. (For interpretation of the references to color in this figure legend, the reader is referred to the web version of the article.)

Please cite this article in press as: F.G. Petzold, et al., Nickel supported on zinc oxide nanowires as advanced hydrodesulfurization catalysts, Catal. Today (2012), http://dx.doi.org/10.1016/j.cattod.2012.05.030

coated on the ZnO NWs, high resolution TEM images were obtained. The TEM images (not shown here) show NiO nano-particles are coated onto ZnO NWs with some NiO particles exhibiting diameters of less than 7 nm. To confirm that the NPs on top of the ZnO NWs are in fact NiO a part of a single ZnO NW was mapped via EDS. The elemental maps shown in Fig. S5 reveal that the ZnO NW is decorated with NiO NPs.

The surface area of 20 m^2/g obtained from BET measurements is in agreement with other publications and simple geometric estimations. The specific surface area could further be improved by using lower diameter ZnO NW. For example, the ZnO NW powders possible with our reactor can have diameters below 10 nm and the estimated surface areas can exceed 70 m^2/g. BET surface areas were also measured for the NiAc sample with the alumina binder and the NiFt sample without binder. The results were 65 and 28 m^2/g, respectively.

3.4. Desulfurization testing

The catalyst sample was prepared with 15% Ni loaded onto 65% ZnO NW powders mixed with γ-alumnia powder and tested using a diesel feed containing 20 ppm of sulfur (thiophene ~10 ppm; benzo-thiophene ~3 ppm; di-benzo-thiophene ~3 ppm; and other severely sterically hindered di-benzo-thiophenes) and 25% of various aromatic and poly-aromatic compounds. The treated samples at various time scales show a very promising result, i.e. ultra-deep desulfurization with ultra low sulfur over a 12 h period. See photographs of treated diesel as a function of time in Fig. 7. However, the performance at steady state is lower than expected and that of state of the art catalysts.

The sulfur content in the product samples was analyzed with an Antek 9000 elemental sulfur analyzer. The sulfur uptake capacity of the Ni/ZnO NW/Al_2O_3 catalyst looks encouraging (see Fig. 7). Sulfur in organic sulfur species needs to be catalytically converted to H_2S in order for it to be stored in sulfide form in the catalyst/adsorbent. The fact that there is very little sulfur left in the product initially reveals that the Ni/ZnO NW catalytically breaks down the sulfur species into H_2S which is then adsorbed by the ZnO NWs. Even though the performance levels off relatively quickly, the concept of reactive adsorption was demonstrated.

3.5. Deactivation of Ni/ZnO NW

Post-mortem TEM, EDS, and XRD measurements were performed in order to gain insight on the rapid deactivation, which took place during de-sulfurization. The TEM study of the spent Ni/ZnO NW sample showed significant morphological changes. In particular, the Ni particles dispersed on ZnO NWs were much larger than in the fresh sample, with some of them reaching the size of over 100 nm (see Fig. 8a). Most of the particles were covered with a thick carbon layer like the one shown in the inset of Fig. 8a. High concentration of carbon in this sample was also confirmed by EDS measurements, both performed in TEM and SEM. In addition, nanoprobe-based EDS measurements in TEM, performed on single particles, indicate that these particles are composed of Ni and Zn (see Fig. 8b). This is in excellent agreement with XRD pattern obtained from this sample, which in addition to ZnO shows peaks of NiZn alloy (Fig. 8c). The NiZn phase was more than likely formed during the reduction step, which, considering the nano-sized nature of the particles involved, was probably too hot. Upon initial reflection one would associate the appearance of the NiZn phase as a strong contributor to the overall deactivation of the reactive adsorbent. However, a recent study [5], reporting on the same reactive adsorbent pair (Ni on ZnO), finds a nano-sized NiZn alloy to be highly active for HDS of thiopenes. In their assessment, the NiZn alloy enhances the interaction between Ni and ZnO which could accelerate the sulfur transfer from NiS to ZnO.

The assembled catalyst system (Ni–Al_2O_3–ZnO NW) showed great initial activity and sulfur absorption. However, as the post-mortem characterization also revealed; extensive coking of the catalyst surface quenched all HDS activity eventually. Given the hydrogen atmosphere of 30 bars, the coking phenomenon appears counterintuitive. However, considering the small Ni particle size with projected high activity of the catalyst sample and the high fraction of feed aromatics and poly-aromatics the catalyst likely underwent rapid coke buildup as a result of strong initial adsorption of the polyaromatic fraction. The highly active Ni phase, starved of adsorb-hydrogen, indiscriminately and incompletely hydrogenated adsorbed feed species, especially the aromatic and polyaromatic share. This probably resulted in relatively stable condensed aromatic clusters and possibly other graphite-like structures eventually physically blocking all active Ni sites in a "fouling" manner. Nevertheless, simple adjustments to the initial experimental setup i.e. reduced calcination and reduction temperature, increased hydrogen pressure, polyaromatics free feeds, lower Ni content, promoters, higher surface area, etc. will help to develop a better understanding of the intricacies of the proposed ultra-deep HDS catalyst system.

4. Conclusions

Gas phase oxidation of micron scale zinc powders using oxygen atmospheric plasma flame using 1.5 kW microwave power allowed for production of hundred gram batches of ZnO NW powders with diameters ranging from 5 to 50 nm and lengths varying from 1 to 15 μm. The resulting powders collected from the exhaust flume contained over 90% of nanowires whose lengths exceeded several microns suggesting continuous growth during entrainment. The Ni impregnation of nanowires resulted in much smaller NiO particles compared to ones on corresponding spherical ZnO NPs. In particular, the decomposition of NiFt as precursor allowed for creation of cube-like morphology with dimensions less than 5 nm. The catalysts prepared using Ni NPs supported on ZnO NWs allowed high initial activity toward deep desulfurization but lost significant activity within 16 h. Analysis of the spent catalyst revealed a NiZn alloy phase which probably evolved during the reduction step and that an excessive amount of coking occurred which eventually shut down activity of the catalyst completely. The use of a diesel oil with a significant fraction of aromatics (about 25%) is attributed to the excessive coking observed.

Acknowledgements

Authors gratefully acknowledge support from Sud Chemie, Advanced Energy Materials, LLC for supporting the project. Authors also acknowledge US Department of Energy (DE-EE0003206) for infrastructural support to Conn Center for Renewable Energy Research at University of Louisville. Authors also acknowledge Ms. Swathi Sunkara for help with SEM and XRD studies and Mr. Venkat K. Vendra for in-depth technical discussions discussed in this study.

Appendix A. Supplementary data

Supplementary data associated with this article can be found, in the online version, at http://dx.doi.org/10.1016/j.cattod.2012.05.030.

References

[1] S.A. Ali, S. Ahmed, Fuel Processing Technology 98 (2012) 39–44.
[2] Q. Gao, T. Ofosu, Catalysis Today 164 (2011) 538–543.

[3] T. Fujikawa, H. Kimura, Catalysis Today 111 (2006) 188–193.
[4] H. Farag, I. Mochida, Journal of Colloid and Interface Science 372 (2012) 121–129.
[5] Y. Zhang, Y. Yang, Applied Catalysis B 119 (2012) 13–19.
[6] E. Ito, J.R.V. Veen, Catalysis Today 116 (2006) 446–460.
[7] C. Song, Catalysis Today 86 (2003) 211–263.
[8] A. Stanislaus, A. Marafi, M. Rana, Catalysis Today 153 (2010) 1–68.
[9] P. Biswas, D. Kunzru, International Journal of Hydrogen Energy 32 (2007) 969–980.
[10] A. Chica, S. Sayas, Catalysis Today 146 (2009) 37–43.
[11] V. Fierro, O. Akdim, H. Provendier, C. Mirodatos, Journal of Power Sources 145 (2005) 659–666.
[12] A. Haryanto, S. Fernando, N. Murali, S. Adhikari, Energy and Fuels 19 (2005) 2098–2106.
[13] J. Llorca, N. Homs, J. Sales, P.R. de la Piscina, Journal of Catalysis 209 (2002) 306–317.
[14] H. Muroyama, R. Nakase, T. Matsui, K. Eguchi, International Journal of Hydrogen Energy 35 (2010) 575–1581.
[15] K. Tawara, J. Imai, H. Iwanami, Sekiyu Gakkaishi-J., Japan Petroleum Institute 43 (2000) 105–113.
[16] I. Bezverkhyy, A. Ryzhikov, G. Gadacz, J.P. Bellat, Catalysis Today 130 (2008) 199–205.
[17] J. Costa-Serra, R. Guil-Lopez, A. Chica, International Journal of Hydrogen Energy 35 (2010) 6709–6716.
[18] J. Fan, G. Wang, Y. Sun, C. Xu, H. Zhou, G. Zhou, J. Gao, Industrial and Engineering Chemistry Research 49 (2010) 8450–8460.
[19] L.C. Huang, Z. Qin, G. Wang, M. Du, H. Ge, X. Li, Z. Wu, J.A. Wang, Industrial and Engineering Chemistry Research 49 (2010) 4670–4675.
[20] Y.J. Lee, N.-K. Park, G.B. Han, S.O. Ryu, T.J. Lee, C.H. Chang, Current Applied Physics 8 (2008) 746–751.
[21] A. Ryzhikov, I. Bezverkhyy, J. Bellat, Applied Catalysis B 35 (2008) 6709–6716.
[22] K. Tawara, T. Nishimura, H. Iwanami, T. Nishimoto, T. Hasuike, Industrial and Engineering Chemistry Research 40 (2001) 2367–2370.
[23] J. Zhang, Y. Liu, S. Tian, Y. Chai, C. Liu, Journal of Natural Gas Chemistry 19 (2010) 327–332.
[24] L. Huang, G. Wang, Z. Qin, M. Dong, M. Du, H. Ge, X. Li, Y. Zhao, J. Zhang, T. Hu, J. Wang, Applied Catalysis B 106 (2011) 26–38.
[25] K. Tawara, T. Nishimura, I. Iwanami, Sekiyu Gakkaishi-J., Japan Petroleum Institute 43 (2000) 114–120.
[26] J.F. Da Costa-Serra, R. Guil-Lopez, A. Chica, International Journal of Hydrogen Energy 35 (2010) 6709–6716.
[27] Z.J. Cheng, J. Nan, H.B. Yu, Y.Q. Liu, S. Geng, G.H. Liu, C.G. Liu, Advances in Materials Research 239 (2011) 754–758.
[28] V. Kumar, J.H. Kim, C. Pendyala, B. Chernomordik, M.K. Sunkara, Journal of Physical Chemistry C 112 (2008) 17750–17754.
[29] R.S. Wagner, W.C. Ellis, Applied Physics Letters 89 (1964) 1753975–1753977.
[30] A.M. Morales, C.M. Lieber, Science 279 (1998) 208–211.
[31] M. Meyyappan, M.K. Sunkara, Inorganic Nanowires: Applications, Properties and Characterization, CRC Press, Boca Raton, FL, 2010.
[32] M.K. Sunkara, S. Sharma, US Patent 7,252,811, August 7, 2007.
[33] S. Sharma, M.K. Sunkara, US Patent 6,806,228, September 16, 2003.
[34] M.K. Sunkara, S. Sharma, US Patent 7,182,818, February 27, 2007.
[35] S. Sharma, M.K. Sunkara, Journal of the American Chemical Society 124 (2002) 12288–12293.
[36] M.K. Sunkara, S. Vaddiraju, M. Mozetic, U. Cvelbar, US Patent 7,591,897, September 22, 2009.
[37] A. Gutsch, M. Kramer, G. Michael, H. Muhlenweg, M. Pridohl, G. Zimmerman, Kona 20 (2002) 24–37.
[38] B. Liu, H.C. Zeng, Journal of the American Chemical Society 12 (2003) 4430–4431.
[39] M.P. Zach, K.H. Ng, R.M. Penner, Science 290 (2000) 2120–2123.

Please cite this article in press as: F.G. Petzold, et al., Nickel supported on zinc oxide nanowires as advanced hydrodesulfurization catalysts, Catal. Today (2012), http://dx.doi.org/10.1016/j.cattod.2012.05.030